Precision test of bound-state QED at intermediate *Z* with kaonic neon

Manti S.[1,*] F. Sgaramella[1] L. Abbene[2,1] C. Amsler[3,†] F. Artibani[1,4] M. Bazzi,[1] G. Borghi[5,6] D. Bosnar,[7,1] M. Bragadireanu,[8] A. Buttacavoli,[2,1] M. Carminati[5,6] A. Clozza[1] F. Clozza[1,9] L. De Paolis,[1] R. Del Grande[10,1] K. Dulski,[1,11,12] C. Fiorini[5,6] I. Friščić[7] C. Guaraldo,[1,‡] M. A. Iliescu[1] P. Indelicato[13] M. Iwasaki,[14] A. Khreptak,[11,12,1] J. Marton,[3,15] P. Moskal[11,12] H. Ohnishi[16] K. Piscicchia,[1,17] F. Principato,[2,1] A. Scordo[1] M. Silarski[11] D. Sirghi[17,1,8] F. Sirghi[1,8] M. Skurzok[11,12,1] J. Sommerfeldt[13] A. Spallone,[1] K. Toho,[16,1] L. Toscano,[5,6] O. Vazquez Doce[1] J. Zmeskal,[3,‡] and C. Curceanu[1,8]
(SIDDHARTA-2 Collaboration)
[1]*Laboratori Nazionali di Frascati INFN, Frascati, Italy*
[2]*Department of Physics and Chemistry (DiFC), Emilio Segrè, University of Palermo, Palermo, Italy*
[3]*Stefan Meyer Institute for Subatomic Physics, Vienna, Austria*
[4]*Università degli Studi di Roma Tre, Dipartimento di Fisica, Roma, Italy*
[5]*Politecnico di Milano, Dipartimento di Elettronica, Informazione e Bioingegneria, Milano, Italy*
[6]*INFN Sezione di Milano, Milano, Italy*
[7]*Department of Physics, Faculty of Science, University of Zagreb, Zagreb, Croatia*
[8]*IFIN-HH, Institutul National Pentru Fizica si Inginerie Nucleara Horia Hulubei, 30 Reactorului, 077125, Magurele, Romania*
[9]*Università degli Studi di Roma Tor Vergata, Dipartimento di Fisica, Roma, Italy*
[10]*Faculty of Nuclear Sciences and Physical Engineering, Czech Technical University in Prague, Břehová 7, 115 19, Prague, Czech Republic*
[11]*Faculty of Physics, Astronomy, and Applied Computer Science, Jagiellonian University, Kraków, Poland*
[12]*Center for Theranostics, Jagiellonian University, Krakow, Poland*
[13]*Laboratoire Kastler Brossel, Sorbonne Université, CNRS, ENS-PSL Research University, Collège de France, Case 74; 4, place Jussieu, F-75005 Paris, France*
[14]*RIKEN, Tokyo, Japan*
[15]*Atominstitut, Technische Universität Wien, Stadionallee 2, 1020 Vienna, Austria*
[16]*Research Center for Accelerator and Radioisotope Science (RARiS), Tohoku University, Sendai, Japan*
[17]*Centro Ricerche Enrico Fermi, Museo Storico della Fisica e Centro Studi e Ricerche "Enrico Fermi," Roma, Italy*

(Received 25 August 2025; accepted 30 January 2026; published 19 February 2026)

We report Dirac-Fock calculations of transition energies for kaonic neon. For the most intense line, the 7–6 transition, the calculated energy is 9450.28 eV, which includes a bound-state quantum electrodynamics (BSQED) contribution of 12.66 eV. This is in excellent agreement with the recent SIDDHARTHA-2 measurement at DAΦNE of $9450.23 \pm 0.37\,(\text{stat.}) \pm 1.50\,(\text{syst.})$ eV. With the quantum electrodynamics contribution far exceeding experimental uncertainty, these results establish kaonic atoms as sensitive platforms for precision tests of BSQED in intermediate-Z systems.

DOI: 10.1103/rry5-tdqb

I. INTRODUCTION

Quantum electrodynamics (QED) is the most accurate theory describing the interaction between charged particles and photons within the framework of quantum field theory. For instance, in the context of bound-state QED (BSQED) [1,2], which utilizes QED to describe interactions in bound atomic systems, theoretical predictions achieve parts-per-billion (ppb) accuracy for the 2S–1S transition in hydrogen [3]. However, for intermediate and high atomic numbers (Z), the theoretical calculations face limitations in reaching similar precision, as the perturbative expansion scales with (αZ), with α the fine-structure constant, leading to convergence issues for high-Z elements. To explore the intermediate-Z case, tests of BSQED are typically conducted using highly charged ions (HCIs) [4–6] confined in cyclotrons and ion traps, enabling the exploration of QED effects in strong electric fields [7]. Nevertheless, for many experimentally accessible transitions, nuclear structure effects, such as the finite nuclear size (FNS), are comparable in magnitude to the higher-order QED contributions and can limit the achievable accuracy, particularly at intermediate Z [8]. Recently, a paradigm shift has occurred

*Contact author: simone.manti@lnf.infn.it
†Present address: Marietta Blau Institute for Particle Physics, Austrian Academy of Sciences, 1010 Vienna, Austria.
‡Deceased.

in BSQED tests at intermediate Z, favoring the use of exotic atoms [9]. These systems, where a negatively charged exotic particle (e.g., μ^-, $\bar{p}$, K^-, π^-) replaces an electron, enable probing regions closer to the nucleus due to the larger mass of the exotic particle compared to the electron, where BSQED effects are highly enhanced [10]. Historically, studies of exotic atoms were constrained to solid targets [11], where electron refilling effects often left residual electrons bound to the atom, complicating the interpretation of spectroscopic data [12]. Recent advancements in detection and accelerator technologies have enabled investigations using low-pressure gas targets, significantly reducing electron refilling [13–17] and allowing for cleaner observations of atomic transitions [18–20]. To date, BSQED tests in exotic atoms have predominantly utilized muonic, pionic, and antiprotonic atoms [9]. In contrast, negatively charged kaons present unique advantages for such studies [21]. Being spin-0 particles, kaons exhibit a strongly reduced hyperfine splitting, unlike muons, simplifying the spectral analysis. Additionally, having an intermediate mass between that of pions, muons, and antiprotons, kaons could provide for BSQED studies a more complete picture across the entire mass range. Moreover, specific transitions within the kaonic atom cascade can be selected to minimize the influence of FNS effects and residual electrons. A notable challenge in employing kaons for precision measurements is the "kaon-mass problem." Several discrepancies exist among measurements of the kaon mass [22–25], with the primary disagreement occurring between the two most precise results [26,27]. This has led to a persistent uncertainty of approximately 30 parts per million (ppm), as reported by the Particle Data Group (PDG) [28]. Resolving this issue is crucial for enhancing the accuracy of BSQED tests involving kaonic atoms. The majority of these studies were conducted prior to 1990, when accurate methods, particularly for addressing electron screening effects, were not yet well established. Nowadays, state-of-the-art multiconfiguration Dirac-Fock (MCDF) methods [29] offer the possibility to take into account all the different effects, potentially uniquely linking and determining the kaon mass from the experiment. Recently, the SIDDHARTA-2 Collaboration at the DAΦNE collider of the National Laboratories of Frascati (INFN-LNF) in Italy, in preparation for the subsequent measurement on kaonic deuterium, successfully performed high-precision x-ray spectroscopy measurements of kaonic neon (KNe with K for K^-) [18] using a gaseous target. This system exhibits several transitions with high yields (>30%) in the x-ray range corresponding to high-n levels. Thanks to the performed optimization and the use of silicon drift detectors (SDDs) [30], sub-eV precision was achieved on the measurement of those lines. In this paper we perform a more refined data analysis and compare the recent SIDDHARTA-2 KNe measurements [18] with state-of-the-art MCDF calculations. We demonstrate excellent agreement between experiment and theory, underscoring the sensitivity of KNe transitions, and kaonic atoms more broadly, to BSQED effects. We also validate the result against the electron screening effect and kaon-mass dependence, and finally show that KNe offers a viable route to refining the charged kaon mass with high precision.

II. METHODS

KNe data were recorded during the 2023 SIDDHARTA-2 run at the DAΦNE [31–33] collider at INFN-LNF. The sample used in this article corresponds to an integrated luminosity of 150 pb^{-1}, representing a 20% increase in statistics compared to our previous result [18]. Further experimental details on the SIDDHARTA-2 setup and KNe measurement are provided in Refs. [34] and [18], respectively. To extract the transition energies from the x-ray spectrum, we performed a maximum likelihood fit in which the observed spectral peaks were modeled using Gaussian functions. Each Gaussian function was explicitly parameterized by the SDDs resolution, incorporating both the Fano factor and electronic noise, consistent with the methodology described in our previous study [30]. Unlike the analysis in Ref. [18], here we explicitly account for the presence of different neon isotopes (^{20}Ne and ^{22}Ne) and model the lines 7i-6h, 8k-7i, and 9l-8k using a Gaussian function for each isotope. The amplitudes of the two components were constrained based on the natural isotopic abundances of neon [35], namely, a ^{22}Ne / ^{20}Ne ratio of 9.78%. The inclusion of ^{21}Ne, which has a natural abundance of 0.27%, as well as the uncertainty in the isotopic abundance ratios, does not affect the fit results within the sensitivity of this study. Systematic uncertainties on the experimental transition energies arise from both the energy stability over time and the calibration procedure, as previously described [36]. To compute the x-ray transition energies, we utilized the Multiconfiguration Dirac-Fock General Matrix Elements (MCDFGME) code (version 2025.1) developed by Desclaux and Indelicato [4,29,37], with the 2018 CODATA fundamental constants [38]. For each transition the code solves the Klein-Gordon equation for both initial and final states of the kaonic atom, and QED contributions are evaluated with vacuum polarization at all-order [39,40]. In all calculations, we consider only transitions between high-n circular states ($\ell = n - 1$). FNS effects are neglected by adopting the point-nucleus approximation, as their impact on transition energies is limited to a few meV, as reported in the Supplemental Material [41]. Recoil corrections are evaluated as in Ref. [42] and included to the transition energies. Electron screening effects are evaluated by including a single electron in the 1s orbital of Ne, constructing the total wave function from the electron and kaon. Unless otherwise specified, we adopt the reference kaon mass from the PDG [28] of $M_{K^-} = 493.677$ MeV. The MCDFGME calculations were used to further constrain the fit of the neon isotopic peaks: the centroid of the K^{22}Ne peak was fixed to the isotopic shift predicted by the calculation, similar to μNe [19], and the resolution of the peak was scaled accordingly. We validated this approach by assessing the change of the isotopic shifts for our lines of interest (7i-6h, 8k-7i, 9l-8k) to variations of the kaon mass w.r.t. the PDG value and found that changing the kaon mass by ±100 keV (more than seven times the current PDG uncertainty) leads to a shift of less than 10 meV (see Fig. 1) in the isotopic shift values. This confirms the robustness of our spectral modeling to fit different isotopic contributions.Radiative and Auger transition rates were calculated using the hydrogenic wave functions and standard analytical formulas widely used

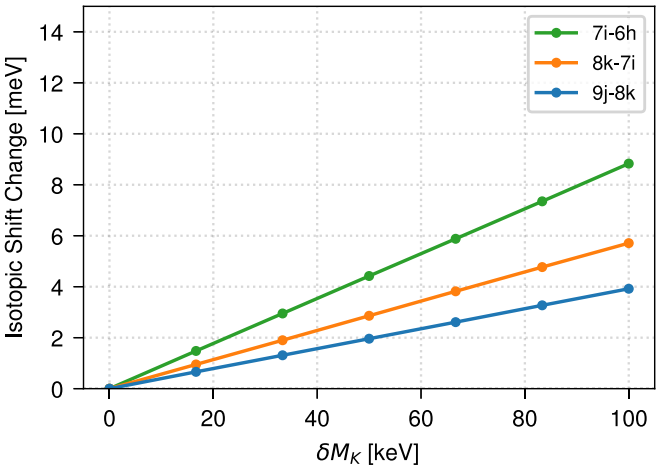

FIG. 1. Change of the isotopic energy shifts as a function of the kaon mass w.r.t. the PDG value for the 7i-6h, 8k-7i, and 9l-8k transitions in $K^{20}Ne$. The maximum variation over the ±100-keV range is 9 meV for 7i-6h, 6 meV for 8k-7i, and 4 meV for 9l-8k.

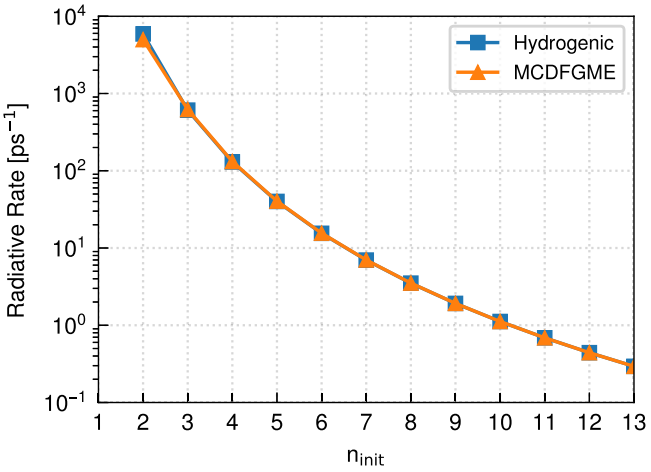

FIG. 2. Comparison of radiative transition rates between circular states in KNe calculated with the scaled hydrogenic formula [43] (blue) and by using MCDFGME wave functions (orange).

in exotic atom studies [43]:

$$\Gamma^{(R)}_{n,l\to n',l\pm1} = \frac{4\mu Z^4}{3}\alpha^3\left|R^{n,l}_{n',l\pm1}\right|^2(\Delta E_{if})^3$$

$$\Gamma^{(A)}_{n,l\to n',l\pm1} = \frac{16}{3}\left(\frac{Z_e}{Z}\right)^2\frac{\pi}{\mu^2}\frac{l}{2l+1}\left|R^{n,l}_{n',l\pm1}\right|^2 \times \frac{y^2}{1+y^2}\frac{\exp[y(4\tan^{-1}y-\pi)]}{\sinh(\pi y)}. \quad (1)$$

The Auger rate formula applies for an electron in the $1s$ orbital, and $Z_e = Z - 1$. ΔE_{if} is the transition energy for the hydrogenic case and $R^{n,\,l}_{n',\,l\pm1}$ is the dipole radial integral, μ denotes the reduced mass of the $K^{20}Ne$ system, and $y = \sqrt{k/2E}$ is the momentum of the ejected K-shell electron. While the development of a dedicated MCDFGME treatment for Auger transitions is planned for future work, we validate the hydrogenic approach by comparing dipole radiative rates from the hydrogenic approximation and MCDFGME calculations. In Fig. 2 the radiative rate from formula 1 is compared with the MCDFGME result for KNe, and for high-n transitions ($n > 5$) the relative error is found to be below 1%. Additionally, to further highlight the potential of KNe measurement, we extract the kaon mass directly from the measured x-ray transitions. This is accomplished by iteratively adjusting the kaon mass in the theoretical calculation until agreement with the experimental value is achieved, following the method of Gall *et al.* [27]. Here, we terminated the iterative procedure once the kaon mass change between successive steps fell below 0.5 keV.

III. RESULTS AND DISCUSSION

We now report the experimental KNe transition energies measured by SIDDHARTA-2 and compare them with the MCDFGME calculations. We then discuss the significance of these results for BSQED studies and their implications for a precise determination of the kaon mass.

A. KNe spectrum

The experimental KNe spectrum, shown in Fig. 3, features three dominant peaks corresponding to the 7–6, 8–7, and 9–8 transitions, observed at approximately 9.4, 6.1, and 4.2 keV, respectively. In addition, several lower-intensity peaks are present which include transitions with $\Delta n > 1$, such as 10–8, 11–9, 12–9, and 12–8. The spectrum also reveals x-ray lines from other kaonic atoms formed in the setup environment, including carbon, oxygen, nitrogen, and titanium. A distinct peak at 10.8 keV is attributed to the bismuth Lα transition, originating from bismuth in the SDD ceramic materials [30]. The identification and relative intensities of these contaminant lines are consistent with our previous observations [36], and their contributions have been carefully included in the analysis. The observed KNe transitions are consistent with expectations based on the competition between radiative and Auger decay channels during the cascade, as shown in Fig. 4. A qualitative analysis of the calculated rates predicts at which levels of the cascade radiative transitions begin to dominate over Auger processes. Specifically, for KNe, radiative decay becomes the dominant channel, starting from an initial principal quantum number of approximately $n_{\text{init}} = 9$ of the cascade (see Fig. 4). Transitions originating from levels below this threshold begin to appear in the spectrum, marking the progressive dominance with increasing yield of radiative emission over Auger deexcitation. A fit was performed to extract the transition energies of the observed peaks (see Fig. 3). The fitting procedure was refined relative to our previous study [18] to enable a direct comparison with theory, specifically by decoupling the contributions from the two neon isotopes (^{20}Ne and ^{22}Ne). Due to the high yield a tail function to the 7–6 line was added, with tail parameters fixed from our previous work [36]. A linear background model was adopted, since more complex forms did not yield a significant improvement in the reduced chi-squared value. Isotopic peaks corresponding to the same transition were constrained to improve fit stability, as detailed in the Methods section. Results for the principal KNe transitions are reported in Table I, with their statistical and systematic uncertainties. The value

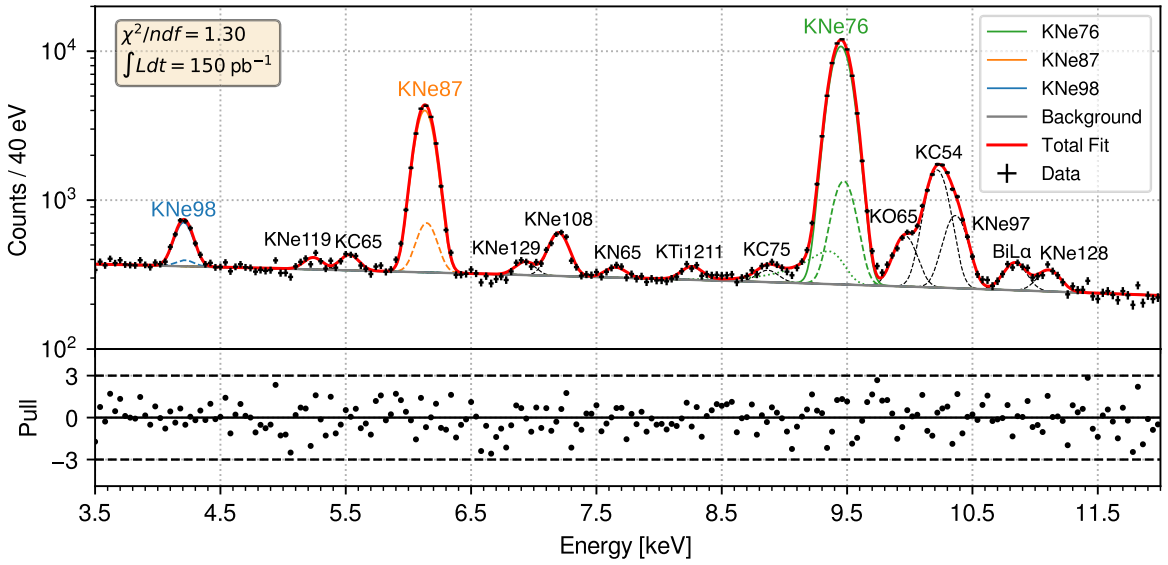

FIG. 3. Fit of the KNe x-ray spectrum (top panel) in the 3.5–12 keV range, showing the counts (black), the total fit (red), individual peak contributions (dashed black), and the background (gray). The main lines of KNe are highlighted: KNe76 (green), KNe87 (orange), and KNe98 (blue), each exhibiting a double component due to the presence of two different neon isotopes (^{20}Ne and ^{22}Ne). For the KNe76 peak, the tail contribution is also shown. The pull plot (bottom panel) displays the fit residuals normalized by the count errors.

for 6h-5g reported in [18] is also included in the table for completeness and as a reference for the calculations.

B. BSQED

We performed MCDFGME calculations to compare the experimentally measured transition energies with theoretical predictions. As summarized in Table I, the calculated transition energies, $E_{if}^{(\mathrm{calc.})}$, are presented alongside additional theoretical contributions. Specifically, we report QED contribution $E_{if}^{(\mathrm{QED})}$ to the transition energies, the sum of the first-order $E_{if}^{(\mathrm{QED1})}$ and second-order $E_{if}^{(\mathrm{QED2})}$ contributions [4].

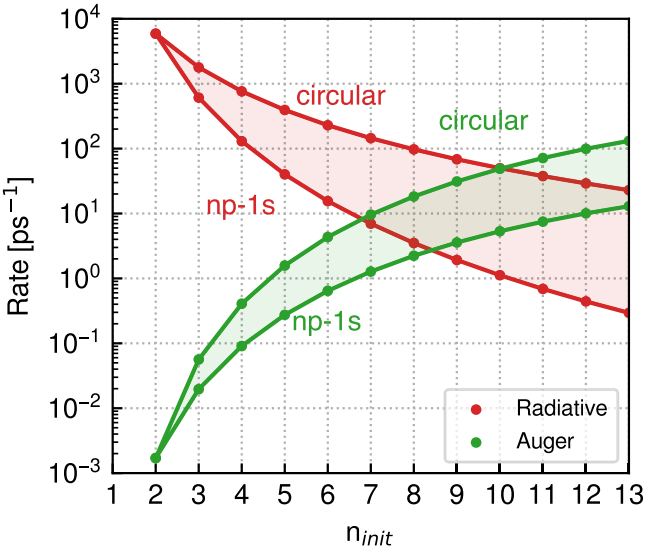

FIG. 4. Radiative and Auger transition rates for KNe as a function of the initial principal quantum number n. Rates for circular ($\ell = n - 1$) and $np \to 1s$ transitions are plotted as lines, while intermediate transitions fall in the corresponding shaded regions.

Accounting for vacuum polarization diagrams at all-order produces no noticeable effect on the transitions analyzed in this work. We also provide the isotopic shift for each transition, $\Delta E_{if}^{(\mathrm{isot.})}$, which was used to constrain the fitting procedure. For the most precisely measured line, the 7–6, we find $E_{76}^{(\mathrm{exp.})} = 9450.23 \pm 0.37\ (\mathrm{stat.}) \pm 1.50\ (\mathrm{syst.})\ \mathrm{eV}$, which is in excellent agreement with the calculated value of $E_{76}^{(\mathrm{calc.})} = 9450.28\ \mathrm{eV}$, where the QED contribution to the transition energy is 12.66 eV. The accuracy of the calculations depends solely on nuclear uncertainties, which have a negligible effect for these high-n transitions, as reported in the Supplemental Material [41], where results for different neon isotopes are reported in the Table S1 of the Supplemental Material [41]. We validate these results against the estimation of the energy shift $\Delta E_{if}^{(\mathrm{screen.})}$ due to the screening effect of an electron in the $1s$ orbital of neon. This contribution, always negative, reflects the reduced effective nuclear charge experienced by the kaon. The precise electron configuration of the atom at the moment of the x-ray transition is not known, since most electrons are expelled during the initial part of the cascade, first from the L shell, then from the K shell [44]. For all studied transitions, electron screening effects were found to be below 1 eV, with the 7–6 line shifted by only $-0.18\ \mathrm{eV}$. However, at the stage when radiative transitions become dominant ($n < 9$), KNe is expected to be highly ionized, as similarly indicated by the cascade calculations performed for KN [45]. This is further supported by the fact that, for these states, the wave functions are well contained within the Ne $1s$ electron orbital (see Fig. 5), indicating that the atom is expected to be highly ionized and therefore electron screening does not limit the comparison between the QED contribution and experiment. These findings establish KNe as a highly effective tool for probing BSQED, owing to its pronounced sensitivity to the magnitude of QED effects. To further establish the suitability of KNe, and kaonic atoms in general, for BSQED studies, we

TABLE I. Experimental transition energies $E_{if}^{(\mathrm{exp.})}$ for KNe obtained from the fit, including their statistical $\delta E_{if}^{(\mathrm{stat.})}$ and systematic $\delta E_{if}^{(\mathrm{sys.})}$ uncertainties, along with the calculated values $E_{if}^{(\mathrm{calc.})}$. The table also shows the QED contributions $E_{if}^{(\mathrm{QED})}$, isotopic $\Delta E_{if}^{(\mathrm{isot.})}$, and electron screening energy shifts $\Delta E_{if}^{(\mathrm{screen.})}$, not included in $E_{if}^{(\mathrm{calc.})}$), and uncertainty due to the PDG kaon mass $\Delta E_{if}^{(\mathrm{PDG})}$. All energies are given in eV.

Transition	$E_{if}^{(\mathrm{exp.})}$	$\delta E_{if}^{(\mathrm{stat.})}$	$\delta E_{if}^{(\mathrm{sys.})}$	$E_{if}^{(\mathrm{calc.})}$	$E_{if}^{(\mathrm{QED})}$	$E_{if}^{(\mathrm{QED1})}$	$E_{if}^{(\mathrm{QED2})}$	$\Delta E_{if}^{(\mathrm{isot.})}$	$\Delta E_{if}^{(\mathrm{screen.})}$	$\Delta E_{if}^{(\mathrm{PDG})}$
9l-8k	4206.97	3.43	2.00	4201.45	2.09	2.07	0.02	9.90	−0.38	0.11
8k-7i	6130.57	0.65	1.50	6130.31	5.09	5.05	0.04	14.45	−0.27	0.16
7i-6h	9450.23	0.37	1.50	9450.28	12.66	12.56	0.10	22.28	−0.18	0.24
6h-5g[a]	15673.30	0.52	9.00	15685.39	32.75	32.51	0.24	37.01	−0.11	0.40

[a]Reference [18].

performed a systematic set of calculations for multiple transitions in KNe up to $n = 15$. Figure 6 provides an overview of the QED contributions across a range of transitions, emphasizing both the sub-eV precision attainable with SDD detectors and the relevant energy window from 2 to 50 keV for the SIDDHARTA-2 experiment. The survey reveals a variety of QED contributions, with transitions such as 7–6 and 6–5 being particularly prominent. Notably, there are several additional transitions with $\Delta n = 1, 2, 3$ where transitions with second-order QED contributions of the order of the sub-eV precision are highlighted. Therefore, performing BSQED studies with kaonic atoms offers several advantages. For kaonic neon, the BSQED contribution to the 7i–6h transition amounts to 12.66 eV, corresponding to about 0.13% of the total transition energy, which is approximately one order of magnitude larger than in the muonic case [19]. As a result, BSQED effects in kaonic atoms can be resolved with higher statistical significance for a given experimental precision. In antiprotonic neon [9], although the larger mass further enhances QED contributions, the interpretation is limited by comparatively larger FNS effects, whose uncertainties reduce the achievable sensitivity to BSQED.

C. Kaon mass

We now investigate the impact of the 13-keV PDG kaon mass uncertainty on the size of the BSQED contributions on the KNe lines. We performed several MCDFGME calculations of the transition lines under examination, scaling for the value of the kaon mass. In Fig. 7 we vary the kaon mass by 50 keV with respect to the PDG value and report the variation of the transition energies. Only positive mass variations are shown, as we find the energy-mass relation to be linear at the ppm scale, while the BSQED contribution shows a dependence on the kaon mass more than two orders of magnitude smaller. Employing the 13-keV uncertainty from PDG, the theoretical uncertainties in transition energies are listed in the last column of Table I. Taken together, these results allow us to summarize the overall theoretical accuracy of the present calculations. For the high-n circular transitions considered here, finite nuclear size and recoil corrections are negligible, at the level of a few meV. Electronic screening effects, while not included in the calculated transition energies, were explicitly evaluated and conservatively treated as a systematic uncertainty below the eV level. The dominant theoretical uncertainty source arises from the present uncertainty on the charged kaon mass, which propagates to 0.24 eV for the 7–6 transition. This total theoretical uncertainty remains well below the experimental

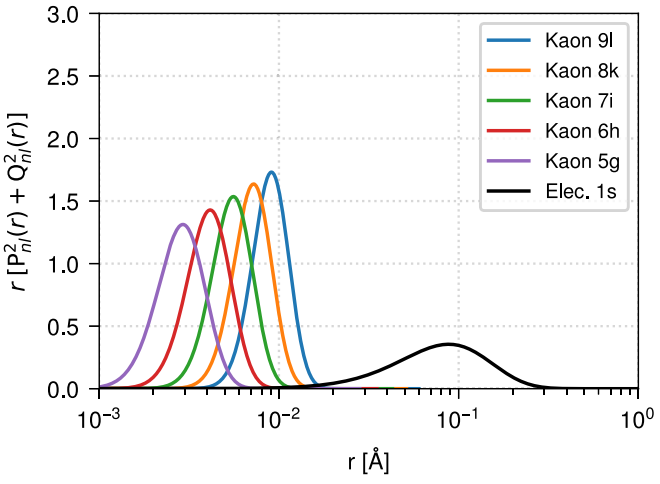

FIG. 5. Radial probability densities for selected kaonic neon states (9l, 8k, 7i, 6h, 5g) compared with the electron 1s wave function of neon. The kaonic wave functions are entirely contained within the electron 1s shell, demonstrating that the kaon orbits deep inside the electronic cloud.

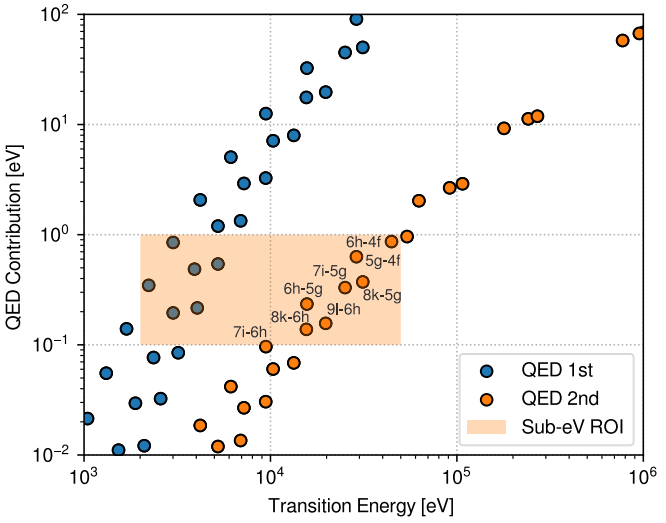

FIG. 6. First-order (blue) and second-order (orange) QED contributions as a function of transition energy for $K^{20}Ne$, all in eV. The sub-eV ROI highlights the region sensitive to the SDDs for transition energies in the 2–50 keV range and precisions in the 0.1–1 eV region.

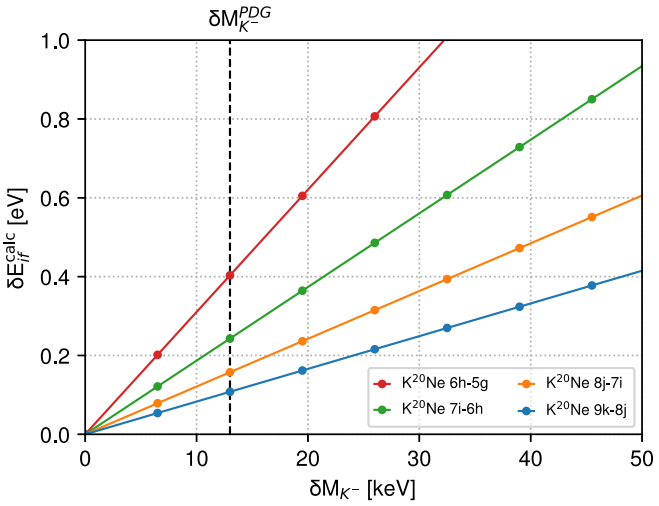

FIG. 7. Variation of the transition energies as a function of the kaon mass. The vertical dashed line indicates the current PDG uncertainty of 13 keV on the kaon mass.

systematic uncertainty and is more than an order of magnitude smaller than the corresponding BSQED contribution. Finally, we show the kaon mass uncertainty achievable with the sub-eV-precision 7–6 and 8–7 transitions of KNe. For each transition we applied the iterative procedure of Gall [27], with full propagation of both statistical and systematic uncertainties. Table II presents the resulting mass values and uncertainties for the 7–6 and 8–7 and their combination.

IV. CONCLUSIONS

In summary, the comparison of state-of-the-art MCDFGME calculations with recent SIDDHARTA-2 measurements at DAΦNE establishes kaonic atoms as a robust platform for testing BSQED in intermediate-Z systems. From the KNe x-ray spectrum fit, we extracted transition energies for the 7–6, 8–7, and 9–8 lines. The 7–6 and 8–7 transitions achieved sub-eV statistical precision, with the 7–6 line measured at 9450.23 ± 0.37 (stat.) $\pm$ 1.50 (syst.) eV, close to the MCDFGME prediction of 9450.28 eV, which includes a QED contribution of 12.66 eV. We also examined two potential systematic effects in the calculations: electron screening and the charged kaon mass uncertainty. For these transitions, the atom is expected to be highly ionized; however, electron screening from a residual 1s electron in neon introduces a shift of only about 1% of the QED contribution. Moreover, the current PDG uncertainty of 13 keV on the kaon mass induces only a few percent variation on transition energies. Together, these findings highlight that theoretical uncertainties remain at the percent level relative to the dominant QED contribution, making kaonic atoms well suited systems for precision BSQED tests in the intermediate-Z regime. In the end, we have shown that by combining the sub-eV-precision 7–6 and 8–7 transitions, it is possible to achieve a statistical uncertainty on the kaon mass below 20 keV, already approaching the precision of the two most accurate, but mutually inconsistent, measurements reported by the PDG. We note that the present experimental setup was optimized for the deuterium measurement; a dedicated campaign focused on kaonic neon could bring the total uncertainty on the kaon mass below 10 keV. This would be achievable by reducing systematic uncertainties through dedicated calibration of the KNe lines at 6 and 9 keV. Additionally, doubling the statistics and optimizing the kaon stopping efficiency specifically for a neon gas target would further lower the statistical uncertainty, potentially reaching the sub-10-keV level. Our results establish KNe as a benchmark for future BSQED tests and for improved determinations of fundamental hadronic properties. Further advances in detector technology and statistics, development of more refined cascade models, and the extension of this methodology to other intermediate-Z kaonic atoms promise even more stringent tests of QED in strong fields. Such progress will enable improved determinations of fundamental particle properties, including the charged kaon mass, and may shed light on discrepancies in precision spectroscopy, hadronic interactions, and the interplay between QED and the strong force in exotic atoms.

TABLE II. Kaon mass (M_{K^-}) extracted from different transitions, along with statistical ($\delta M_{K^-}^{\text{stat.}}$) and systematic ($\delta M_{K^-}^{\text{syst.}}$).

Transition	M_{K^-} [MeV]	$\delta M_{K^-}^{\text{stat.}}$ [keV]	$\delta M_{K^-}^{\text{syst.}}$ [keV]
7i-6h	493.674	19	78
8k-7i	493.699	52	121
7i-6h + 8k-7i	493.677	18	66

ACKNOWLEDGMENTS

We thank C. Capoccia from INFN-LNF and H. Schneider, L. Stohwasser, and D. Pristauz-Telsnigg from Stefan Meyer-Institut for their fundamental contribution in designing and building the SIDDHARTA-2 setup. We also thank INFN-LNF and the DAΦNE staff for the excellent working conditions and their ongoing support. Special thanks to Catia Milardi for her continued support and contribution during the data taking. We gratefully acknowledge Polish high-performance computing infrastructure PLGrid (HPC Center: ACK Cyfronet AGH) for providing computer facilities and support within Computational Grant No. PLG/2025/018524. Part of this work was supported by the INFN (KAONNIS Project); the Austrian Science Fund (FWF): [P24756-N20 and P33037-N]; the Croatian Science Foundation under Project No. IP-2022-10-3878; the EU STRONG-2020 project (Grant Agreement No. 824093); the EU Horizon 2020 project under the MSCA (Grant Agreement No. 754496); the Japan Society for the Promotion of Science JSPS KAKENHI Grants No. JP18H05402 and No. JP22H04917; the Polish Ministry of Science and Higher Education under Grant No. 7150/E-338/M/2018 and the Polish National Agency for Academic Exchange (Grant No. PPN/BIT/2021/1/00037); the EU Horizon 2020 research and innovation program under project OPSVIO (Grant Agreement No. 101038099).

DATA AVAILABILITY

The data that support the findings of this article are openly available [46], embargo periods may apply.

[1] P. Indelicato, in *Atomic Physics with Heavy Ions*, edited by H. F. Beyer and V. P. Shevelko (Springer, Berlin, Heidelberg, 1999), pp. 92–116.

[2] P. Indelicato and P. J. Mohr, in *Handbook of Relativistic Quantum Chemistry* (Springer, Berlin, Heidelberg, 2016), pp. 1–110.

[3] C. G. Parthey, A. Matveev, J. Alnis, B. Bernhardt, A. Beyer, R. Holzwarth, A. Maistrou, R. Pohl, K. Predehl, T. Udem, *et al.*, Phys. Rev. Lett. **107**, 203001 (2011).

[4] P. Indelicato, J. Phys. B: At. Mol. Opt. Phys. **52**, 232001 (2019).

[5] V. M. Shabaev, A. I. Bondarev, D. A. Glazov, M. Y. Kaygorodov, Y. S. Kozhedub, I. A. Maltsev, A. V. Malyshev, R. V. Popov, I. I. Tupitsyn, and N. A. Zubova, Hyperfine Interact. **239**, 60 (2018).

[6] J. Morgner, B. Tu, C. M. König, T. Sailer, F. Heiße, H. Bekker, B. Sikora, C. Lyu, V. A. Yerokhin, Z. Harman, *et al.*, Nature (London) **622**, 53 (2023).

[7] J. Ullmann, Z. Andelkovic, C. Brandau, A. Dax, W. Geithner, C. Geppert, C. Gorges, M. Hammen, V. Hannen, S. Kaufmann, *et al.*, Nat. Commun. **8**, 15484 (2017).

[8] A. V. Volotka, D. A. Glazov, G. Plunien, and V. M. Shabaev, Ann. Phys. **525**, 636 (2013).

[9] N. Paul, G. Bian, T. Azuma, S. Okada, and P. Indelicato, Phys. Rev. Lett. **126**, 173001 (2021).

[10] D. Gotta, Prog. Part. Nucl. Phys. **52**, 133 (2004).

[11] B. Jeckelmann, T. Nakada, W. Beer, G. de Chambrier, O. Elsenhans, K. L. Giovanetti, P. F. A. Goudsmit, H. J. Leisi, A. Rüetschi, O. Piller, *et al.*, Phys. Rev. Lett. **56**, 1444 (1986).

[12] L. M. Simons, D. Abbot, B. Bach, R. Bacher, A. Badertscher, P. Blüm, P. DeCecco, J. Eades, J. Egger, K. Elsener, *et al.*, Nucl. Instrum. Methods Phys. Res., Sect. B **87**, 293 (1994).

[13] R. Bacher, P. Blüm, D. Gotta, K. Heitlinger, M. Schneider, J. Missimer, and L. M. Simons, Phys. Rev. A **39**, 1610 (1989).

[14] K. Kirch, D. Abbott, B. Bach, P. Hauser, P. Indelicato, F. Kottmann, J. Missimer, P. Patte, R. T. Siegel, L. Simons, *et al.*, Phys. Rev. A **59**, 3375 (1999).

[15] S. Lenz, G. Borchert, H. Gorke, D. Gotta, T. Siems, D. F. Anagnostopoulos, M. Augsburger, D. Chatellard, J. P. Egger, D. Belmiloud, P. El-Khoury, P. Indelicato, M. Daum, P. Hauser, K. Kirch, and L. M. Simons, Phys. Lett. B **416**, 50 (1998).

[16] M. Trassinelli, D. F. Anagnostopoulos, G. Borchert, A. Dax, J.-P. Egger, D. Gotta, M. Hennebach, P. Indelicato, Y.-W. Liu, B. Manil, N. Nelms, L. M. Simons, and A. Wells, EPJ Web Conf. **130**, 01022 (2016).

[17] M. Trassinelli, D. F. Anagnostopoulos, G. Borchert, A. Dax, J. P. Egger, D. Gotta, M. Hennebach, P. Indelicato, Y. W. Liu, B. Manil, N. Nelms, L. M. Simons, and A. Wells, Phys. Lett. B **759**, 583 (2016).

[18] F. Sgaramella, D. Sirghi, K. Toho, F. Clozza, L. Abbene, C. Amsler, F. Artibani, M. Bazzi, G. Borghi, D. Bosnar, *et al.*, Phys. Lett. B **865**, 139492 (2025).

[19] T. Okumura, T. Azuma, D. A. Bennett, I. Chiu, W. B. Doriese, M. S. Durkin, J. W. Fowler, J. D. Gard, T. Hashimoto, R. Hayakawa, *et al.*, Phys. Rev. Lett. **130**, 173001 (2023).

[20] T. Okumura, T. Azuma, D. A. Bennett, W. B . Doriese, M. S. Durkin, J. W. Fowler, J. D. Gard, T. Hashimoto, R. Hayakawa, Y. Ichinohe, *et al.*, Phys. Rev. Lett. **134**, 243001 (2025).

[21] C. Curceanu, C. Guaraldo, M. Iliescu, M. Cargnelli, R. Hayano, J. Marton, J. Zmeskal, T. Ishiwatari, M. Iwasaki, S. Okada, *et al.*, Rev. Mod. Phys. **91**, 025006 (2019).

[22] G. Backenstoss, A. Bamberger, I. Bergström, T. Bunaciu, J. Egger, R. Hagelberg, S. Hultberg, H. Koch, Y. Lynen, H. G. Ritter, *et al.*, Phys. Lett. B **43**, 431 (1973).

[23] L. M. Barkov, I. B. Vasserman, M. S. Zolotorev, N. I. Krupin, S. I. Serednyakov, A. N. Skrinsky, V. P. Smakhtin, E. P. Solodov, G. M. Tumaikin, Y. M. Shatunov, *et al.*, Nucl. Phys. B **148**, 53 (1979).

[24] S. C. Cheng, Y. Asano, M. Y. Chen, G. Dugan, E. Hu, L. Lidofsky, W. Patton, C. S. Wu, V. Hughes, and D. Lu, Nucl. Phys. A **254**, 381 (1975).

[25] G. K. Lum, C. E. Wiegand, E. G. Kessler, R. D. Deslattes, L. Jacobs, W. Schwitz, and R. Seki, Phys. Rev. D **23**, 2522 (1981).

[26] A. Denisov, A. Zhelamkov, Y. Ivanov, L. Lapina, M. Levchanko, V. Malakhov, A. Petrunin, A. Sergeev, A. Smirnov, V. Suvorov, *et al.*, JETP Lett. **54**, 558 (1991).

[27] K. P. Gall, E. Austin, J. P. Miller, F. O'Brien, B. L. Roberts, D. R. Tieger, G. W. Dodson, M. Eckhause, J. Ginkel, P. P. Guss, *et al.*, Phys. Rev. Lett. **60**, 186 (1988).

[28] S. Navas, C. Amsler, T. Gutsche, C. Hanhart, J. Hernández-Rey, C. Lourenço, A. Masoni, M. Mikhasenko, R. Mitchell, Patrignani, *et al.*, Phys. Rev. D **110**, 030001 (2024).

[29] J. V. Mallow, J. P. Desclaux, and A. J. Freeman, Phys. Rev. A **17**, 1804 (1978).

[30] M. Miliucci, A. Scordo, D. Sirghi, A. Amirkhani, A. Baniahmad, M. Bazzi, D. Bosnar, M. Bragadireanu, M. Carminati, M. Cargnelli, *et al.*, Meas. Sci. Technol. **32**, 095501 (2021).

[31] C. Milardi, D. Alesini, S. Bini, O. R. Blanco-García, M. Boscolo, B. Buonomo, S. Cantarella, S. Caschera, A. De Santis, G. Delle Monache, *et al.*, in *Proceedings of 9th International Particle Accelerator Conference (IPAC'18), Vancouver, BC, Canada* (JACOW Publishing, Geneva, Switzerland, 2018), pp. 334–337.

[32] C. Milardi, D. Alesini, O. R. Blanco-García, M. Boscolo, B. Buonomo S. Cantarella, A. De Santis, C. Di Giulio, G. Di Pirro, A. Drago, *et al.*, in *Proceedings of 12th International Particle Accelerator Conference (IPAC2021), Campinas, SP, Brazil* (JACOW Publishing, Geneva, Switzerland, 2021), pp. 1322–1325.

[33] C. Milardi, D. Alesini, O. Blanco-García, M. Boscolo, B. Buonomo, S. Cantarella, J. Chavanne, A. D'Uffizi, A. De Santis, C. Di Giulio, *et al.*, in *Proceedings of 15th International Particle Accelerator Conference (IPAC'24)* (JACoW Publishing, Geneva, Switzerland, 2024), pp. 2504–2507.

[34] F. Sirghi, M. Iliescu, L. Abbene, C. Amsler, M. Bazzi, G. Borghi, D. Bosnar, M. Bragadireanu, A. Buttacavoli, M. Carminati, *et al.*, J. Instrum. **19**, P11006 (2024).

[35] G. Audi, A. H. Wapstra, and C. Thibault, Nucl. Phys. A **729**, 337 (2003), The 2003 NUBASE and Atomic Mass Evaluations.

[36] F. Sgaramella, M. Tüchler, C. Amsler, M. Bazzi, D. Bosnar, M. Bragadireanu, M. Cargnelli, M. Carminati, A. Clozza, G. Deda, *et al.*, Eur. Phys. J. A **59**, 56 (2023).

[37] J. P. Santos, F. Parente, S. Boucard, P. Indelicato, and J. P. Desclaux, Phys. Rev. A **71**, 032501 (2005).

[38] E. Tiesinga, P. J. Mohr, D. B. Newell, and B. N. Taylor, Rev. Mod. Phys. **93**, 025010 (2021).

[39] J. M. Schmidt, G. Soff, and P. J. Mohr, Phys. Rev. A **40**, 2176 (1989).
[40] G. Soff and P. J. Mohr, Phys. Rev. A **38**, 5066 (1988).
[41] See Supplemental Material at http://link.aps.org/supplemental/10.1103/rry5-tdqb for extended tables of transition energy calculations.
[42] M. Trassinelli and P. Indelicato, Phys. Rev. A **76**, 012510 (2007).
[43] G. R. Burbidge and A. H. de Borde, Phys. Rev. **89**, 189 (1953).
[44] V. R. Akylas and P. Vogel, Comput. Phys. Commun. **15**, 291 (1978).
[45] T. Koike, in *2nd International Conference on Exotic Atoms and Related Topics* (Austrian Academy of Sciences Press, Wien, Germany, 2005), pp. 215–219.
[46] S. Manti, Precision test of bound-state QED at intermediate Z with kaonic neon [Data set], Zenodo (2026), https://doi.org/10.5281/zenodo.18619466.